Inorganic Chemistry

Article

pubs.acs.org/IC

Role of the Acceptor in Tuning the Properties of Metal [M(II) = Ni, Pd, Pt] Dithiolato/Dithione (Donor/Acceptor) Second-Order Nonlinear Chromophores: Combined Experimental and Theoretical Studies

Davide Espa,[†] Luca Pilia,[‡] Christodoulos Makedonas,[§] Luciano Marchiò,[∥] M. Laura Mercuri,[†] Angela Serpe,[†] Alberto Barsella,[⊥] Alain Fort,[⊥] Christiana A. Mitsopoulou,*[,§] and Paola Deplano*[,†]

[†]Dipartimento di Scienze Chimiche e Geologiche, Università di Cagliari, S.S. 554-Bivio per Sestu, I09042 Monserrato-Cagliari, Italy

[‡]Dipartimento di Ingegneria Meccanica, Chimica e dei Materiali, Università di Cagliari, via Marengo 2, I09123 Cagliari, Italy

[§]Chemistry Department, Inorganic Laboratory, National and Kapodistrian University of Athens, Panepistimiopolis, Zografou, 15 771 Greece

[∥]Dipartimento di Chimica, Università di Parma, Parco Area delle Scienze 17A, I43100 Parma, Italy

[⊥]Département d'Optique ultra-rapide et Nanophotonique, IPCMS-CNRS, 23 Rue du Loess, BP 43, 67034 Strasbourg Cedex 2, France

Supporting Information

ABSTRACT: The mixed-ligand complexes [M(II)(Et_2dazdt)(mnt)] (M = Ni, **1**; Pd, **2**; Pt, **3**) [Et_2dazdt = *N*,*N*′-diethylperhydrodiazepine-2,3-dithione; mnt = maleonitrile-2,3-dithiolate] have been prepared and fully characterized. X-ray diffractometric studies on **1**−**3** (the structure of **1** was already known) show that the crystals are isostructural (triclinic, *P*−1), and two independent molecular entities are present in the unit cell. These entities differ in the orientation of the ethyl substituents with respect to the epta-atomic ring. In the $C_2S_2MS_2C_2$ dithiolene core the four sulfur atoms define a square-planar coordination environment of the metal where the M−S bond distances involving the two ligands are similar, while the C−S bond distances in the C_2S_2 units exhibit a significant difference in Et_2dazdt (dithione) and mnt (dithiolato) ligands. **1**−**3** show in the visible region one or two moderately strong absorption peaks, having ligand-to-ligand charge-transfer (CT) character with some contribution of the metal, and show negative solvatochromism and molecular quadratic optical nonlinearity, which was determined by the EFISH (electric-field-induced second-harmonic generation) technique. These complexes are redox active and show two reversible reduction waves and one irreversible oxidation wave. Theoretical calculations based on DFT and TD-DFT calculations on complexes **1**−**3** as well as on [Pt(Bz_2pipdt)(mnt)] (**4**) and [Pt(Bz_2pipdt)(dmit)] (**5**) highlight the factors which affect the optical properties of these second-order redox-active NLO chromophores. Actually, the torsion angle of the dithione system (δ_2) inversely correlates either with the oscillator strengths of the main transition of the complexes or with their beta values. The high beta value of **5** can be attributed both to its lowest torsion angles and to the extent of the π system of its dithiolate ligand, dmit.

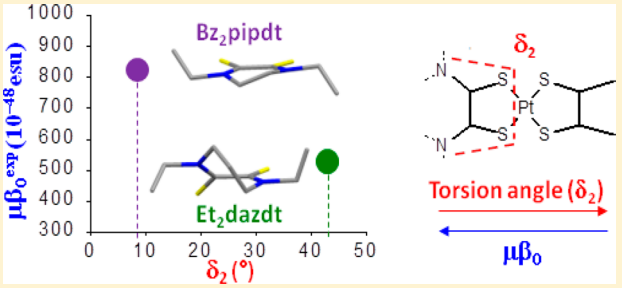

INTRODUCTION

Complexes of d^8 metals with noninnocent ligands based on donor−acceptor systems, are of current interest for their peculiar electronic properties which make them suitable for potential use in advanced technologies such as photocatalysts,[1] in solar energy harnessing,[2] and as second-order nonlinear chromophores.[3] In square-planar d^8-metal dithiolene complexes, terminal groups attached to the dithiolene core ($C_2S_2MC_2S_2$) and having different donor/acceptor properties induce a redistribution of the π electrons in such a way that one of the ligands can be described as a dithione (acceptor) and the other one as a dithiolato (donor).[4] These asymmetric complexes can generate second-order NLO properties at the molecular level, while a noncentrosymmetric crystal packing is also required for a bulk material.[3] It has been found that square-planar d^8-metal mixed-ligand dithiolenes are characterized by the presence of a solvatochromic absorption in the visible−near-infrared spectral region and show remarkably high negative molecular first hyperpolarizability.[5] The solvatochromic peak is relatable to a HOMO−LUMO transition, where the HOMO is formed by a mixture of metal and dithiolate orbitals while the dithione orbitals give a predominant contribution to the LUMO. A mixed metal/ligand to ligand charge-transfer character (MMLL′CT) has been assigned to this transition.[6] A systematic study on varying the *metal*,[6] *donor*,[7] and *acceptor* ligands is performed to

Received: November 4, 2013
Published: January 9, 2014

   dx.doi.org/10.1021/ic402738b | *Inorg. Chem.* 2014, 53, 1170−1183

highlight the role that each of them plays in tuning the properties of these complexes. Combined theoretical and experimental studies have allowed us to point out the role of the metal and donor ligands. In particular, in the triad [M(II)(Bz$_2$pipdt)(mnt)] (M(II) = Ni, Pd, and Pt; Bz$_2$pipdt =1,4-dibenzyl-piperazine-2,3-dithione; mnt = maleonitriledithiolato) it is shown that the most appealing candidate is the platinum compound.[6] This is relatable to (i) the most extensive mixture of the dithione/metal/dithiolato orbitals in the frontier orbitals (FOs), (ii) the influence of the electric field of the solvent on the FOs that maximizes the difference in dipole moments between excited and ground states, and (iii) the largest oscillator strength of the platinum compound.

The present study allows us to deepen the factors which affect the properties of these chromophores to highlight, in particular, the role of the acceptor. For this purpose, experimental and theoretical studies have been performed on the title complexes which are compared to similar systems bearing the same dithiolato ligand (mnt) and differing for the dithione one, which for the sake of clarity are depicted in Chart 1.

Chart 1

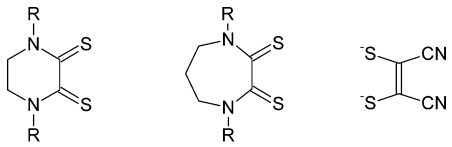

EXPERIMENTAL SECTION

General Comments. Reagents and solvents of reagent grade and spectroscopic grade (DMF, CH_3CN, and CS_2) have been used as received from Aldrich. When not available reagents Et$_2$dazdt,[7] [Ni(Et$_2$dazdt)$_2$](BF$_4$)$_2$,[5] [Pd(Et$_2$dazdt)Cl$_2$], and [Pt(Et$_2$dazdt)Cl$_2$][6,8,9] were prepared following already described procedures. Microanalyses were performed by means of a Carlo Erba CHNS Elemental Analyzer model EA1108.

Synthesis and Characterization. *[Ni(Et$_2$dazdt)(mnt)] (**1**).* [Ni(Et$_2$dazdt)$_2$](BF$_4$)$_2$ (118.5 mg, 0.19 mmol) was dissolved in CH_3CN (25 cm^3), and (*n*-Bu$_4$N)$_2$[Ni(mnt)$_2$] (157.5 mg, 0.19 mmol) in CH_3CN (20 cm^3) was added dropwise. The mixture was refluxed for 10 min, yielding a deep green solution and a black precipitate. Precipitate was removed by centrifugation, and crude product was recrystallized from CH_3CN/Et_2O. Yield: 146.3 mg (0.35 mmol), 92%. Analytical results are in accordance with the formula [Ni(Et$_2$pipdt)(mnt)]. Anal. Found (calcd for $C_{13}H_{16}N_4NiS_4$): C, 37.5 (37.6); H, 3.9 (3.8); N, 13.3 (13.5); S, 30.5 (30.9). FT-IR (cm^{-1}): 2976 w, 2934 w, 2870 w, 2200 s, 1523 vs, 1483 m, 1452 m, 1443 m, 1358 w, 1344 w, 1285 w, 1236 w, 1153 w, 1123 w, 984 w, 789 w, 735 w, 509 w. UV−vis (in CH_3CN), λ/nm (ε/dm^3 mol^{-1} cm^{-1}): 601 (2.4 × 10^3), 818 (1.9 × 10^3).

*[Pd(Et$_2$dazdt)(mnt)] (**2**).* A MeOH solution of Na$_2$mnt (37.5 mg, 0.20 mmol in 10 cm^3) was added dropwise to a DMF solution of [Pd(Et$_2$dazdt)Cl$_2$] (78.7 mg, 0.20 mmol in 20 cm^3), and the mixture was left under stirring for 30 min (50 °C). MeOH was rotary evaporated, and a dark-green solid precipitated after diethyl ether addition. Following centrifugation, the solution was removed and the solid recovered. Recrystallization of the crude product from DMF/Et_2O gave 80.5 mg (0.17 mmol), in 87% yield. Analytical results are in accordance with the formula [Pd(Et$_2$dazdt)(mnt)]. Anal. Found (calcd for $C_{13}H_{16}N_4PdS_4$): C, 33.5 (33.7); H, 3.7 (3.5); N, 11.8 (12.1); S, 26.9 (27.1). FT-IR (cm^{-1}): 2977 w, 2933 w, 2872 w, 2331 m, 2205 s, 1522 s, 1487 m, 1456 m, 1385 s, 1362 w, 1343 m, 1281 m, 1234 w, 1148 w, 1123 w, 982 w, 789 w, 679 w, 507 w. UV−vis (in DMF), λ/nm (ε/dm^3 mol^{-1} cm^{-1}): 356 (5.1 × 10^3), 485 (1.3 × 10^3), 670 (1.0 × 10^3).

*[Pt(Et$_2$dazdt)(mnt)] (**3**).* This compound was prepared as described for **2** starting from [Pt(Et$_2$dazdt)Cl$_2$] (67.5 mg; 0.14 mmol) in DMF and Na$_2$mnt (27.5 mg; 0.13 mmol) in MeOH. Yield: 69.5 mg (0.14 mmol), 90% (black crystals). Different solvents are used due to the different solubility of reagents. Anal. Found (calcd for $C_{13}H_{16}N_4PtS_4$): C, 28.1 (28.3); H, 3.1 (2.9); N, 10.0 (10.2); S, 23.0 (23.2). FT-IR (cm^{-1}): 2978 w, 2933 w, 2872 w, 2368 w, 2338 w, 2205 s, 1520 vs, 1485 m, 1454 s, 1364 s, 1344 m, 1285 s, 1238 s, 1155 s, 1121 w, 1090 w, 982 w, 790 m, 735 w, 510 w. UV−vis (in DMF), λ/nm (ε/dm^3 mol^{-1} cm^{-1}): 331 (16.4 × 10^3), 401 (7.0 × 10^3), 680 (7.1 × 10^3).

Spectroscopic Measurements. IR spectra (4000−350 cm^{-1}) were recorded on a Bruker IFS55 FT-IR Spectrometer as KBr pellets. Electronic spectra were recorded with a Cary 5 spectrophotometer. Cyclic voltammograms were carried out on a EG&G (Princeton Applied Research) potentiostat-galvanostat model 273 using a conventional three-electrode cell consisting of a platinum wire working electrode, a platinum wire as counter-electrode, and Ag/AgCl in saturated KCl solution as reference electrode. Experiments were performed at room temperature (25 °C) in dry and argon-degassed DMF containing 0.1 mol dm^{-3} Bu$_4$NBF$_4$ as supporting electrolyte, at 25−200 mV s^{-1} scan rate. Half-wave potential for ferrocene/ferrocenium couple (internal standard) is +0.43 V under the above conditions.

EFISH experiments were performed using a freshly prepared 10^{-3} M solution in DMF and working with a 1907 nm incident wavelength, obtained by Raman shifting the 1064 nm emission of a Q-switched Nd:YAG laser in a high-pressure hydrogen cell (50 bar). The solution is placed in a cell with thick windows in the wedge configuration in order to obtain the Maker fringe pattern (harmonic intensity variation as a function of the beam propagation length in the liquid). In the EFISH experiments the incident pulses (7 ns duration) are synchronized with a dc field applied to the solution in order to break its centrosymmetry (2−4 μs pulse duration). From the concentration dependence of the amplitude of the harmonic signal with respect to that of the pure solvent, the NLO responses have been determined (assumed to be real because the imaginary part has been neglected) from the experimental value γ_{EFISH} through eq 1

$$\gamma_{EFISH} = \frac{\mu\beta_\lambda(-2\omega;\ \omega,\ \omega)}{5kT} + \gamma(-2\omega;\ \omega,\ \omega,\ 0) \qquad (1)$$

where γ_{EFISH} is the sum of a cubic electronic contribution $\gamma(-2\omega;\ \omega,\ \omega,\ 0)$ and of a quadratic orientational contribution $\mu\beta_\lambda\ (-2\omega;\ \omega,\ \omega)/5kT$, where μ is the ground state dipole moment and β_λ the projection along the dipole moment direction of the vectorial component β_{vec} of the tensorial quadratic hyperpolarizability at wavelength λ.

X-ray Crystallography. A summary of data collection and structure refinement for **1**−**3** is reported in Table 1. Single-crystal data were collected with a Bruker Smart APEXII (**1** and **2**) and Bruker AXS Smart 1000 (**3**) area detector diffractometers. All data collection were performed with Mo Kα radiation (λ = 0.71073 Å). Cell constants were obtained using 60 ω frames of 0.5° width and scanned from three different zones of reciprocal lattice. Intensity data were integrated from several series of exposures frames (0.3° width) covering the sphere of reciprocal space.[10] Absorption corrections were applied using the program SADABS[11] with min and max transmission factors of 0.803−1.000 (**1**), 0.797−1.000 (**2**), and 0.481−1.000 (**3**). Structures were solved by direct methods (SIR97[12] and SIR2004[13]) and refined on F^2 with full-matrix least-squares (SHELXL-97[14]) using the Wingx software package.[15] Non-hydrogen atoms were refined anisotropically for all compounds, and hydrogen atoms were placed at their calculated positions. Graphical material was prepared with the ORTEP3 for Windows[16a] and Mercury CSD 3.1[16b] programs. CCDC 930260(**2**) and 930261(**3**) contain supplementary crystallographic data for this paper.

Hirshfeld surface (HS) analysis[17a] was performed on the two molecules that comprise the asymmetric unit of **1**−**3** in order to gain

dx.doi.org/10.1021/ic402738b | Inorg. Chem. 2014, 53, 1170−1183

Table 1. Summary of X-ray Crystallographic Data for [M(II)(Et_2dazdt)(mnt)] 2 (M = Pd) and 3 (M = Pt)

	2	3
empirical formula	$C_{26}H_{32}N_8Pd_2S_8$	$C_{26}H_{32}N_8Pt_2S_8$
fw	952.88	1103.26
color, habit	dark green, plate	black, plate
cryst size, mm	0.18 × 0.14 × 0.03	0.45 × 0.20 × 0.08
cryst syst	triclinic	triclinic
space group	*P*−1	*P*−1
a, Å	8.957(3)	8.994(2)
b, Å	9.332(3)	9.354(2)
c, Å	24.143(7)	24.146(6)
α, deg	89.521(4)	89.730(4)
β, deg	87.520(4)	87.220(5)
γ, deg	66.342(4)	66.290(4)
V, Å^3	1847(1)	1857.5(7)
Z	2	2
T, K	293(2)	293(2)
ρ(calcd), Mg/m^3	1.665	1.973
μ, mm^{-1}	1.457	8.003
θ range, deg	0.84−23.31	0.84−27.20
no. of reflns/obsd	16 722/5303	21 833/8131
GooF	1.002	1.004
$R1^a$	0.0596	0.0431
$wR2^a$	0.0783	0.0793

$^aR1 = \Sigma||F_o| - |F_c||/\Sigma|F_o|$, $wR2 = [\Sigma[w(F_o^2 - F_c^2)^2]/\Sigma[w(F_o^2)^2]]^{1/2}$, $w = 1/[\sigma^2(F_o^2) + (aP)^2 + bP]$, where $P = [\max(F_o^2,0) + 2F_c^2]/3$.

insights into the differences between the interactions that each molecule exchanges with the surrounding environment. HS defines the volume of space in a crystal where the sum of the electron density of spherical atom for the molecule (pro-molecule) exceeds that for the crystal (pro-crystal). Various properties of the HS can be computed and visualized, in particular, d_e and d_i, which represent the distance from a point on the surface to the nearest nucleus outside or inside, respectively, the surface. In addition, by combining d_e and d_i with the van deer Waals radii of the atomic species one can define d_{norm}, which provides clear evidence of the interactions occurring between adjacent molecule or molecular fragments that are shorter than the van der Waals radii sum

$$d_{norm} = \frac{d_i - r_i^{vdW}}{r_i^{vdW}} + \frac{d_e - r_e^{vdW}}{r_e^{vdW}}$$

The HS and its properties were calculated with CrystalExplorer 3.0.[17b]

Computational Details. Ground-state electronic structure calculations of complexes **1**−**5** were performed using density functional theory (DFT)[18,19] methods employing the GAUSSIAN 09[20] software packages. The functional used throughout this study was the B3LYP, consisting of a hybrid exchange functional as defined by Becke's three-parameter equation[21] and the Lee−Yang−Parr correlation functional.[22] Full geometry optimization started from structural data under no symmetry constraint.

The basis set employed for nitrogen, carbon, and hydrogen atoms was the well-known valence triple-*ζ* 6-311+G*.[23,24] In the case of sulfur, we used the cc-pVTZ basis set.[25] In addition, we selected the Stuttgart−Dresden effective core potentials for the metal atoms in order to describe the core electrons.[26] ECPs were of the type 60MDF, 28MDF, and 10MDF for Pt, Pd, and Ni, respectively, unless otherwise stated. The latter were complemented by the relative valence triple-*ζ*-quality basis sets.[27−30] Furthermore, the converged wave functions were found free from internal instabilities. Percentage compositions of molecular orbitals were calculated using the AOMix suite of programs.[31,32]

In order to model the compounds' interaction to a solvent's electric field, we employed the polarizable conductor calculation model (CPCM) as implemented in G09.[33,34] Throughout the study we mainly used two solvent fields, chloroform's and acetonitrile's, but since we wanted to describe both complexes' solvation and solvatochromic behavior, we performed relative calculations also in the gas phase and in the more polar solvent DMSO. The 25 lowest singlet excited states of the closed-shell complexes were calculated within the TDDFT formalism as implemented in Gaussian[35] in both an acetonitrile- and a chloroform-simulated electric field, while the percentage of different transitions contributing to a state were calculated with the aid of SWizard.[31,36] The coupled perturbed method was employed to derive the compounds' hyperpolarizabilities based on the Kohn−Sham wave functions. Moreover, calculations were performed in order to obtain *β* off-resonance at 0.65 eV. In both cases the Taylor series convention was employed.[37,38]

Finally, the graphics presented here were drawn with the aid of ChemCraft[39] and Mercury.[40]

RESULTS AND DISCUSSION

Synthetic Procedure. Mixed-ligand complexes [M(II)(Et_2dazdt)(mnt)] (M = Ni, **1**; Pd, **2**; Pt, **3**) [Et_2dazdt = *N*,*N*′-diethyl-perhydrodiazepine-2,3-dithione; mnt = maleonitrile-2,3-dithiolate] are obtained as summarized in Schemes 1 and 2.

Scheme 1

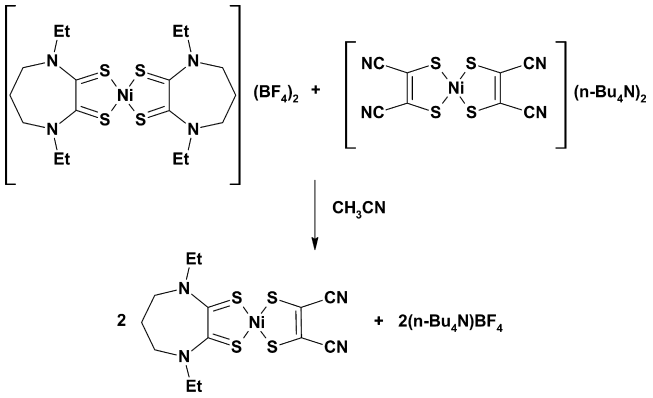

Scheme 2

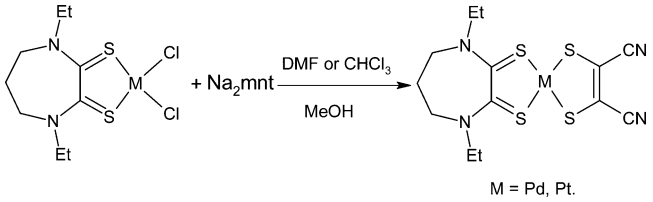

Accordingly **1**, is obtained by mixing CH_3CN solutions of [Ni(Et_2dazdt)$_2$](BF_4)$_2$ and (n-Bu_4N)$_2$[Ni(mnt)$_2$]. Well-formed dark crystals are recovered by slow evaporation of the solvent in high yield.

The corresponding reaction in the palladium and platinum cases does not produce the mixed-ligand complexes but the ion-pair charge-transfer salts [M(Et_2dazdt)$_2$][M(mnt)$_2$].[41a] Similarly, by mixing metal−dithiolate complexes with metal−dithione ones formation of charge-transfer salts between the molecular components has been previously observed in the palladium and platinum cases.[41b,c] The different products obtained by reacting Ni(II) and Pd(II)/Pt(II) corresponding complexes may be relatable to the different inertness of reagents (low in the Ni case) and solubility (low in the Pd and Pt CT salts) of the products. Instead, reacting [M(Et_2dazdt)Cl_2] with a maleonitriledithiolato salt the mixed-ligand Pd (**2**)

dx.doi.org/10.1021/ic402738b | Inorg. Chem. 2014, 53, 1170−1183

and Pt (**3**) complexes are obtained in high yields as shown in Scheme 2 and described in detail in the Experimental Section.

Crystals of **2** and **3** have been obtained as dark-green needles by slow diffusion of diethyl ether into their saturated DMF solution. Crystals of **1**, **2**, and **3** have been used for X-ray diffractometric characterization.

Complexes **1**, **2**, and **3** are characterized in the visible region by two or one broad absorptions with low to medium molar absorption coefficients [**1**, λ/nm (ε/dm^3 mol^{-1} cm^{-1}) 601 (2.4×10^3), 818 (1.9×10^3) in CH_3CN; **2** 670 (1.0×10^3) and **3** 680 (7.1×10^3) in DMF].

All complexes (**1** undergoes transformation in DMF) show negative solvatochromism, which is displayed in Figure 1 for **3**

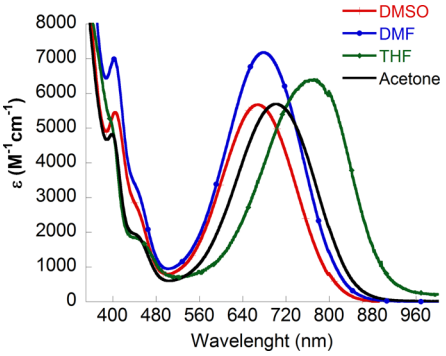

Figure 1. Absorptivities of **3** in different solvents showing the negative solvatochromic behavior.

as an example. The energy of the solvatochromic peak linearly depends on the solvent polarity parameter proposed by Cummings and Eisenberg for d^8-metal diimine−dithiolato complexes,[42a] and the solvatochromic shifts determined as the gradient of this plot [3.6 (**2**) and 4.8 (**3**)] fall in the range found for metal donor−acceptor ligand complexes.[42]

EFISH (electric-field-induced second-harmonic generation) experiments have been performed as described in detail in the Experimental Section. Measurement allows determination of the scalar product $\mu\beta_\lambda$ (μ = ground-tate dipole moment; β_λ = projection of the vectorial component of the quadratic hyperpolarizability tensor along the dipole moment axis). $\mu\beta_\lambda$ values for **2**, -400×10^{-48} esu, and **3**, -1300×10^{-48} esu, determined with an uncertainty of about 10% at 1907 nm incident wavelength, have been extrapolated to zero frequency applying the equation $\beta_0 = \beta_\lambda[1 - (2\lambda_{max}/\lambda)^2][1 - (\lambda_{max}/\lambda)^2]$, obtaining $\mu\beta_0$ values equal to -177×10^{-48} esu for **2** and -576×10^{-48} esu for **3**. A $\mu\beta_\lambda$ value for **1** = -900×10^{-48} esu has been determined in DMF. Degradation of diluted DMF solutions of **1** has been observed. This process is much slower in concentrated solutions, and the observed NLO activity may be ascribed to a no-decomposed fraction of **1**. As previously found, it can be noted that the platinum complex exhibits the largest second-order polarizability in the metal triad. NLO activity is also expected for **1**, **2**, and **3** when embedded in poled polymers but not when they formed pure crystals, since they crystallize in a centrosymmetric space group.

Cyclic voltammetric data of [M(Et$_2$dazdt)(mnt)] are collected in Table 2, where [M(R$_2$pipdt)(mnt)] are also reported for comparison reasons. As shown, two reversible reduction waves (see CV scans of **3** in Figure 2 as an example) and one irreversible oxidation wave, reported as Supporting Information (Figure S1), are exhibited by complexes. A linear dependence

Table 2. Cyclic voltammetric Data[a]

complex	E_a (V) 0 → 1+	$E^1_{1/2}$ (V) 0 ⇆ 1−	$E^2_{1/2}$ (V) 1− ⇆ 2−
[Ni(Et$_2$dazdt)(mnt)][a]	+1.12	−0.53	−0.87
[Pd(Et$_2$dazdt)(mnt)][b]	+1.04	−0.46	−0.78
[Pt(Et$_2$dazdt)(mnt)][b]	+0.96	−0.42	−0.79
[Ni(Bz$_2$pipdt)(mnt)][b]	+1.09	−0.39	−0.90
[Pd(Bz$_2$pipdt)(mnt)[b]	+1.20	−0.35	−0.84
[Pt(Bz$_2$pipdt)(mnt)][b]	+1.08	−0.37	−0.87

[a]Measured at Pt electrode in CH_3CN (superscript a) or DMF (superscript b) solutions, 0.1 M Bu_4NPF_6, scan rate 100 mV/s (reference electrode Ag/AgCl). [M(Bz$_2$pipdt)(mnt)] (M = Ni, Pd, Pt) data are reported for comparison reasons.

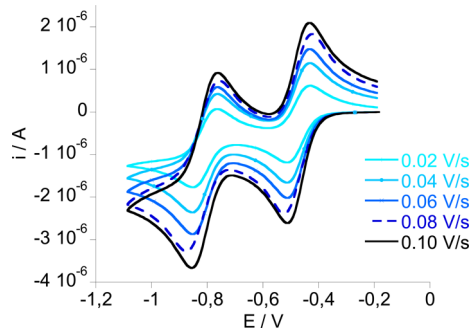

Figure 2. Cyclic voltammograms of **3** recorded at 298 K with different scan rates in DMF solution containing 0.1 M Bu_4NBF_4.

of the peak currents (ip) from the square root of the voltage scan rate has been observed (ip_{red}/ip_{ox} close to the unity) for the reductions peaks. Comparison of **1**−**3** CV data with those the corresponding mixed-ligand complexes bearing R$_2$pipdt[6] shows that the two classes of complexes show a similar behavior, but the sequence of the first reduction process suggests that monoreduction is more difficult in R$_2$dazdt than in R$_2$pipdt derivatives.

A summary of X-ray crystallographic data and selected bond lengths and angles for complexes **1**−**3** are reported in Tables 1 and 3, respectively. It is worth noting that the structure of **1** was already described.[43] Complexes **1**−**3** are isostructural (P−1 space group), and for this reason only the structure of **3** will be described in detail. In Figure 3 the molecular structure of [Pt(Et$_2$dazdt)(mnt)] is depicted. The metal is in a square planar geometry achieved by coordination of two different bidentate sulfur donor ligands. The asymmetric unit comprises two complex molecules that are partially stacked, and the unit containing M(2) (M = Ni, Pd, Pt) exhibits a pronounced distortion from the ideal square planar geometry ranging from 5.7° to 10.2° according to the torsion angle S(Et$_2$dazdt)−S(mnt)−S′(mnt)−S′(Et$_2$dazdt), δ_1 (see Figure 6). Moreover, the diazepane ring adopts a boat conformation. It is the same conformation that is adopted by the azo ring in several other complexes known in the literature.[44−46] It is interesting though that in seven-membered organic rings such as the 1,4-dioxacycloheptane[47] and other heterorings[48−50] it is a twisted chair conformation that lies in the global minimum of the potential energy surface. The two molecular entities of the asymmetric unit differ by the conformation adopted by the ethyl side chain with respect to the coordination plane. In fact, one conformation corresponds to a syn arrangement whereas the second to an anti arrangement (Ni-syn (**1a**), Ni-anti (**1b**); Pd-syn (**2a**), Pd-anti (**2b**); Pt-syn (**3a**), Pt-anti (**3b**)).

dx.doi.org/10.1021/ic402738b | Inorg. Chem. 2014, 53, 1170−1183

Table 3. Selected Bond Lengths (Angstroms) and Angles (degrees) for [M(II)(Et_2dazdt)(mnt)] 1 (M = Ni), 2 (M = Pd), and 3 (M = Pt)

		1	
Ni(1)−S(11)	2.1821(8)	Ni(2)−S(13)	2.1924(7)
Ni(1)−S(21)	2.1932(8)	Ni(2)−S(23)	2.1910(8)
Ni(1)−S(12)	2.1522(8)	Ni(2)−S(14)	2.1425(7)
Ni(1)−S(22)	2.1467(8)	Ni(2)−S(24)	2.1422(7)
C(11)−S(11)	1.694(3)	C(13)−S(13)	1.687(2)
C(21)−S(21)	1.693(3)	C(23)−S(23)	1.694(2)
C(12)−S(12)	1.731(3)	C(14)−S(14)	1.733(3)
C(22)−S(22)	1.731(3)	C(24)−S(24)	1.730(3)
C(11)−C(21)	1.483(3)	C(13)−C(23)	1.489(3)
C(12)−C(22)	1.350(4)	C(14)−C(24)	1.353(3)
S(11)−Ni(1)−S(21)	92.26(3)	S(13)−Ni(2)−S(23)	92.59(3)
S(12)−Ni(1)−S(22)	93.12(3)	S(14)−Ni(2)−S(24)	92.84(3)
		2	
Pd(1)−S(11)	2.310(3)	Pd(2)−S(13)	2.312(3)
Pd(1)−S(21)	2.322(3)	Pd(2)−S(23)	2.312(3)
Pd(1)−S(12)	2.282(3)	Pd(2)−S(14)	2.268(3)
Pd(1)−S(22)	2.265(3)	Pd(2)−S(24)	2.264(3)
C(11)−S(11)	1.683(9)	C(13)−S(13)	1.679(9)
C(21)−S(21)	1.69(1)	C(23)−S(23)	1.68(1)
C(12)−S(12)	1.72(1)	C(14)−S(14)	1.73(1)
C(22)−S(22)	1.72(1)	C(24)−S(24)	1.74(1)
C(11)−C(21)	1.51(1)	C(13)−C(23)	1.52(1)
C(12)−C(22)	1.37(1)	C(14)−C(24)	1.39(1)
S(11)−Pd(1)−S(21)	89.6(1)	S(13)−Pd(2)−S(23)	90.2(1)
S(12)−Pd(1)−S(22)	90.8(1)	S(14)−Pd(2)−S(24)	90.6(1)
		3	
Pt(1)−S(11)	2.299(2)	Pt(2)−S(13)	2.309(2)
Pt(1)−S(21)	2.308(2)	Pt(2)−S(23)	2.308(2)
Pt(1)−S(12)	2.267(2)	Pt(2)−S(14)	2.260(2)
Pt(1)−S(22)	2.264(2)	Pt(2)−S(24)	2.259(2)
C(11)−S(11)	1.709(7)	C(13)−S(13)	1.608(6)
C(21)−S(21)	1.704(7)	C(23)−S(23)	1.701(7)
C(12)−S(12)	1.756(7)	C(14)−S(14)	1.747(7)
C(22)−S(22)	1.746(7)	C(24)−S(24)	1.725(7)
C(11)−C(21)	1.477(9)	C(13)−C(23)	1.507(8)
C(12)−C(22)	1.343(9)	C(14)−C(24)	1.369(9)
S(11)−Pt(1)−S(21)	81.21(7)	S(13)−Pt(2)−S(23)	89.43(6)
S(12)−Pt(1)−S(22)	91.05(7)	S(14)−Pt(2)−S(24)	90.41(7)

Structural differences between the two molecules are not limited to the side chain conformation. If we take into account only the main core of the molecule irrespective of the ethyl positions, the syn arrangement (**3a**) is very close to a C_2 geometry whereas the anti isomer (**3b**) adopts a geometry where the central $-CH_2-$ group of the diazepane lies 0.89 Å out of the Pt−mnt plane (Figure S2, Supporting Information). The latter difference could be attributed to the way the anti molecule interacts with its neighbors. In order to have a thorough description of the environment surrounding the syn and anti arrangements that comprise the asymmetric unit of **1**−**3**, the Hirshfeld surface properties were investigated. According to the HS, it can be appreciated how the hydrogen atoms in the two conformations exchange different contacts. In particular, the methyl group of one of the ethyl residues interacts with different strength with the carbon atom of the dithiolate system ($H_{IN}\cdots C$), and in the syn conformation the interaction appears stronger. These interactions are visualized as red spots on the HS that correspond to the mapping of d_{norm} on the HS,

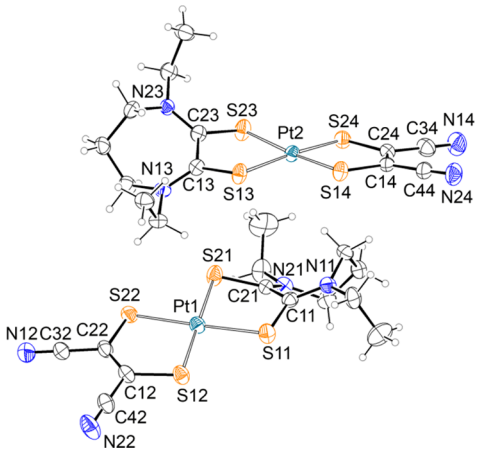

Figure 3. Molecular structure of [Pt(Et_2dazdt)(mnt)] (**3**) with thermal ellipsoids at the 30% probability level. In the unit cell, two independent molecular entities are present, which comprise the Pt(1) and Pt(2) atoms. Compound **3** is isostructural to **1** and **2**.

Figure 4. In addition, a complete depiction of the interaction exchanged by the fragment of the Et_2dazdt ligand comprising the ethyl residues can be obtained by inspecting the fingerprint plots, which are 2D diagrams that provide a clear-cut indication on the subtle differences between similar structural arrangements. By a comparison of Figure 4, Figures S3 and S4, Supporting Information, it can be observed that **1a**−**3a** and **1b**−**3b**, respectively, have nearly identical features, which is nevertheless in agreement with the fact that **1**−**3** are isostructural. On the other hand, the most notable difference between the syn and the anti species is related to the greater strength with which the CH_2 groups of the epta-atomic ring interacts with the surrounding cyano groups in the anti conformation. In the 2D plots this can be evidenced in the more pronounced cusp ($H_{IN}\cdots N_{OUT}$) for the anti conformer when compared to the syn one.

Theoretical Studies. *a. Structural Aspects.* To gain further insight into the structure−property relationships of **1**−**3** theoretical calculations were employed to study their properties. The same computational methods were also employed for the strictly related complex [Pt(Bz_2pipdt)(mnt)] (**4**)[6] and [Pt(Bz_2pipdt)(dmit)] (**5**),[6,9] which exhibits the largest second-order NLO activity so far determined for this class of complexes. Calculated structures of **3a**, **4**, and **5** are depicted in Figure 5, while structural parameters obtained from the optimization procedures for all compounds under study are collected in Tables S1−S4, Supporting Information.

These tables indicate that the calculated M−S bond lengths are systematically slightly overestimated by our calculations, with the binding angles slightly affected as well. This behavior is anticipated and does not have any major impact on the validity of our calculations.[6,19,51] It is worth mentioning though that the agreement of our calculated structures toward the experimental data is better for the less polar solvent employed, chloroform, as compared to acetonitrile. We must also underline the fact that there are some small differences regarding the deduced bond lengths within the first coordination sphere (structures **1a** and **3a** against **1b** and **3b**, e.g., Ni−S (mnt) bond is slightly elongated in the anti conformer). These differences are not reproduced in the calculations, as expected, since in solution the molecules are free from the intermolecular interactions that dominate the crystal structures. Nevertheless, taking all data

dx.doi.org/10.1021/ic402738b | Inorg. Chem. 2014, 53, 1170−1183

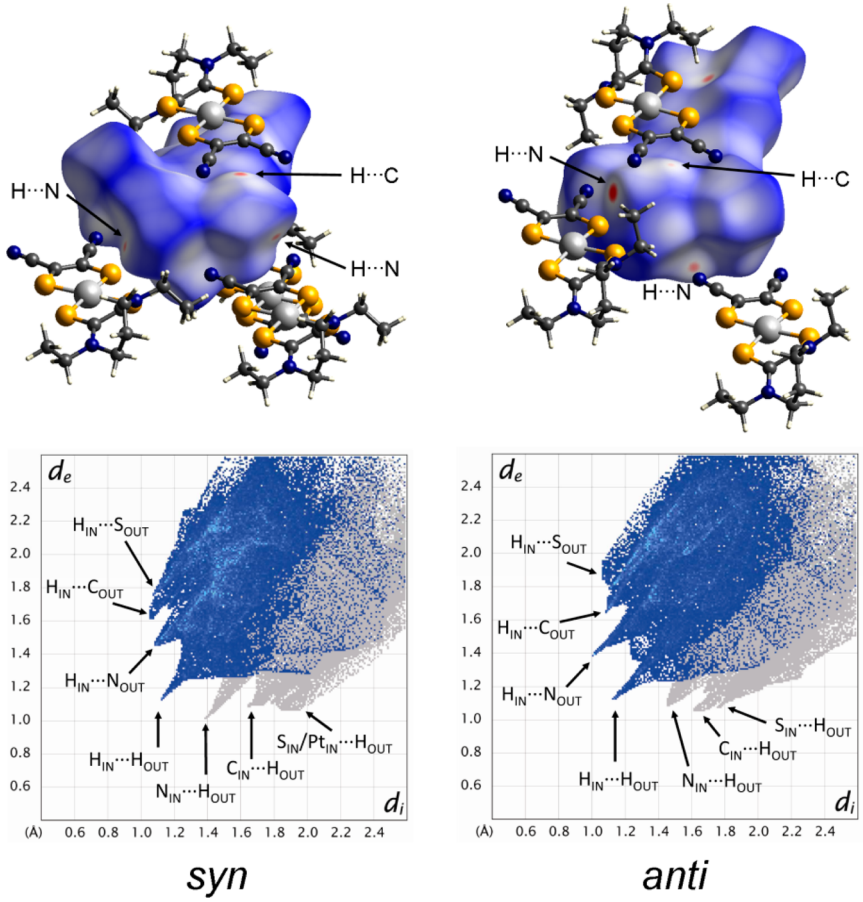

Figure 4. (Top) Depiction of the Hirshfeld surface for the syn and anti conformations of [Pt(Et_2dazdt)(mnt)]; relevant interactions between the hydrogen atom of the surface and the surrounding atoms are evidenced as red spots on the surface. (Bottom) Fingerprint plots depicting the interactions between the two conformers with their surrounding molecules. Blue area corresponds to interactions exchanged between the hydrogen atoms and the surrounding molecules.

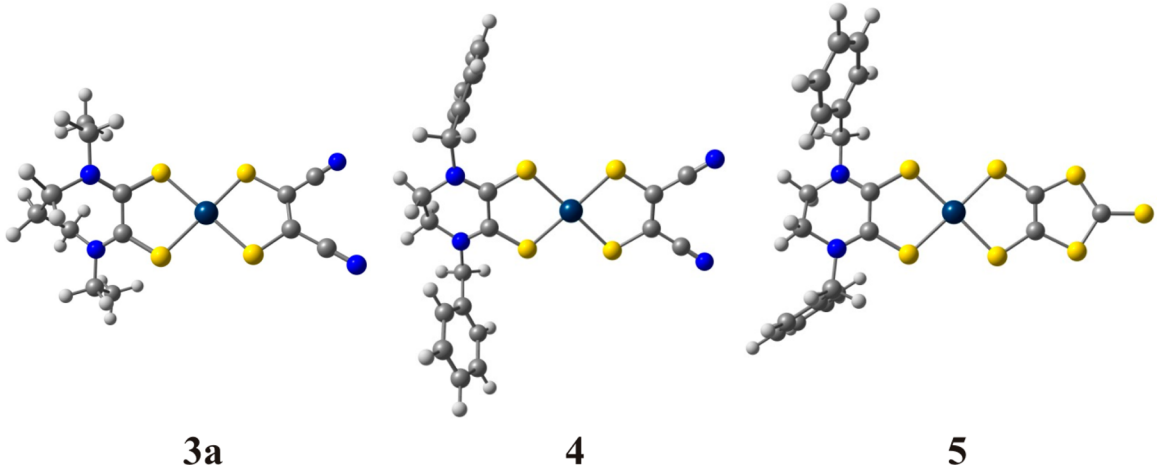

Figure 5. Optimized structures for platinum complexes **3a**, **4**, and **5**.

into consideration, the performance of our model could be judged as quite satisfactory.

In all complexes under study the central metal is coordinated to four sulfur donor atoms in a nearly square planar arrangement. In these compounds, a d^8 metal is coordinated to two ligands with different nature. The first one is a dithione, the 1,4-diethyl-1,4-diazepane-2,3-dithione in the case of **1**−**3** and 1,4-dibenzylpiperazine-2,3-dithione in **4** and **5**, which can be characterized as an electron acceptor, whereas the second ligand, maleonitriledithiolate in **1**−**4** and 2-thioxo-1,3-dithiolane-4,5-dithiolate in **5**, can be characterized as an electron donor. Thus, **1**−**5** belong to the *push*−*pull* type of complexes.

The structures of **1**−**3** deviate from planarity in the ligation sphere according to the values of the torsion angle (δ_1), namely, S(Et_2dazdt)−S(mnt)−S′(mnt)−S′(Et_2dazdt). The largest deviations are observed in **1** (calculated δ_1 for **1a** in

dx.doi.org/10.1021/ic402738b | *Inorg. Chem.* 2014, 53, 1170−1183

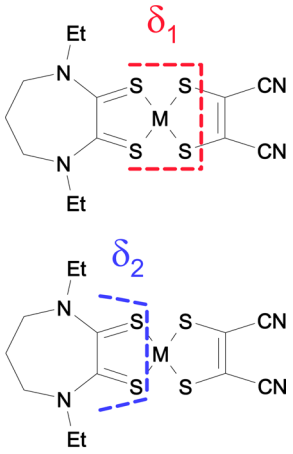

Figure 6. Torsion angles δ_1 and δ_2 defined as indicated by the dot lines.

chloroform' field is 6.2°), while the smallest is observed for **3** in this series of complexes (Figure 6). The aforementioned deviations are even smaller in **4** and **5** (Tables S1−S4, Supporting Information). In complexes **4** and **5**, the dithione moiety is attached to a six-membered azo ring, in contrast to **1**−**3**, where diazepane is a diazocycloheptane. Addition of a methylene group in the six-membered piperazine ring causes the diazepane structure to heavily twist. The N(azo-ring)−S(dithione)−S′(dithione)−N′(azo-ring) torsion angle (δ_2) from a mean value of 2.7° in **4** and **5** becomes ∼40° in **3**. The same situation holds also for **1** and **2** when compared to the corresponding [M(R_2pipdt)(mnt)] complexes[6] and is highest in the palladium complex. Finally, the methylene group of the anti conformer is calculated to lie on the M−mnt plane in structures **1b**, **2b**, and **3b**, in contrast to the X-ray structures (vide supra). In the syn conformers though it seems that a small deviation from planarity exists in solution.

Since there are two stable conformers from each diazepane complex, the syn and anti forms, theoretical calculations were performed for both of them. Computed thermodynamic parameters are collected in Table 4, indicating that since the syn conformer is the most stable one (with the exception of the couple **3a**/**3b** in chloroform) and should prevail in solution. On the other hand, the energy differences calculated are in any case smaller than the thermal barrier ($3/2kT$ = 0.89 kcal/mol at T = 300 K), and hence, both conformers will be present in a solution at room temperature. In the following sections, the aforementioned percentages are taken into account when we refer to calculated values.

Table 4. Gibbs Free Energy Differences between Diazepane Complexes' Conformers

complex	phase/ solvent	conformer	$\Delta\Delta G$ kcal/mol	percentage in a mixture (%)
1	$CHCl_3$	**1a**	0.0	86
	$CHCl_3$	**1b**	1.1	14
	CH_3CN	**1a**	0.0	88
	CH_3CN	**1b**	1.2	12
2	$CHCl_3$	**2a**	0.0	83
	$CHCl_3$	**2b**	1.0	17
	CH_3CN	**2a**	0.0	79
	CH_3CN	**2b**	0.8	21
3	gp	**3a**	0.0	55
	gp	**3b**	0.1	45
	$CHCl_3$	**3a**	0.1	44
	$CHCl_3$	**3b**	0	56
	CH_3CN	**3a**	0.0	71
	CH_3CN	**3b**	0.5	29
	DMSO	**3a**	0.0	70
	DMSO	**3b**	0.5	30

Focusing on the central metal's structural role, it is evident from Tables S1−S3, Supporting Information, that M−S bond lengths are sensitive to the metal. To be more specific, the M−S bond lengths increase in the order Ni−S < Pt−S < Pd−S; a similar trend was observed for the [M(Bz_2pipdt)(mnt)] complexes,[6] in accordance with the smallest bonding radius of Ni and the relativistic effects, which govern the third-row metals and contract several inner orbitals. This trend also agrees with the ionic radii of the d^8 metals (78 pm for Pd(II) and 74 pm for Pt(II)). We should point out that a combination of Dirac−Fock relativistic-type pseudopotentials and valence triple-ζ-quality basis sets to all atoms is necessary in order for this trend to be correctly reproduced. Furthermore, M−S distances in the case of the dithiolate ligand seem to be shorter than the relative distances in the dithione. This fact underlines the difference in bonding between the *push* and the *pull* ligand. Between the two Pt(dithione)(mnt) complexes, **3** and **4**, the M−S(mnt) bond length is slightly larger in **4**, whereas the M−S (dithione) bond length is larger in **3**. In addition, from a comparison between structural data of the two [Pt(Bz_2pipdt)-(dithiolate)] complexes, **4** and **5**, we observe that the M−S-(dithiolate) bond is larger in the case of the dmit ligand, with the M−S(dithione) bond being practically the same. As a result, we can assume that the maleonitriledithiolate ligand is a better acceptor of electron density ligand (and hence should stabilize the HOMO).

For the chelated five-membered dithiolene rings, the C−C and C−S bonds should be indicators of the electronic properties that are induced through complexation. For the *push* 1,2-dithione, the C−C bond is expected to be longer than the relative bond in an electron-accepting *pull* 1,2-dithiolate, while for the C=S bond the trend should be the opposite. Indeed, this is what is observed; the C−C bond distance is ∼1.35 and ∼1.34 Å in mnt and dmit, respectively, whereas this bond is longer in Et_2dazdt and Bz_2pipdt (∼1.50 and ∼1.49 Å, respectively). The same bond is 1.40 Å in benzene. On the other hand, C−S is longer in mnt and dmit and shorter in diazepane and piperazine (∼1.73, ∼1.74, ∼1.70, and ∼1.69 respectively).

b. Electronic Description. The acetonitrile effect modeled by the CPCM procedure is mainly focused on the HOMO−LUMO gap (Figure 7) and on the composition of the frontier orbitals for **1a**−**3a**, **4**, and **5** (Table 5). Details of the ground-state electronic data are provided in Tables S5−S10, Supporting Information. Since complexes **1**−**5** are highly solvatochromic, we performed theoretical calculations employing solvents of different polarity but also calculations in the gas phase in order to investigate changes to their electronic description upon solvation. In this class of complexes it was previously shown that there is an *inverted bonding scheme*,[6,52,53] whereas the HOMO is formed from the out-of-plane antisymmetric interactions between the metal's d_{xz} orbital and a dithiolate based π orbital and the LUMO by antisymmetric interactions between a π-dithione and a metal d orbital.[5,6,8,9,41,51] Although the main trend is similar for **1**−**3**, there is a difference due to the twisting of the dithione ring induced by the diazepane boat

dx.doi.org/10.1021/ic402738b | Inorg. Chem. 2014, 53, 1170−1183

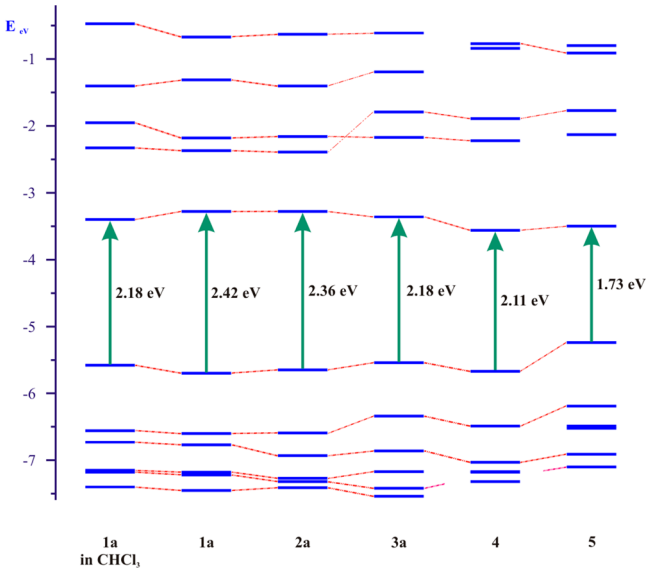

Figure 7. Energy level diagram of **1**−**5**. HOMO−LUMO energy gap is represented by the arrow and value (in eV).

conformation (Tables S1−S3, Supporting Information). This twisting destroys the almost b_1 local symmetry of metal−dithione interactions in the LUMO, which is common for this type of compounds. The situation is identical to both syn and anti conformers. HOMO and LUMO along with the frontier orbitals of **3a** are depicted in Figure 8. Furthermore, there are some minor orbital contributions of dithione in HOMO (9.6%, 8.4%, and 15.1% in **1a**, **2a**, and **3a**, respectively) and dithiolate in LUMO (5.8%, 8.5%, and 5.5% in **1**, **2**, and **3**, respectively). These contributions are consistent with π^*-back-donation theory.[6,51]

LUMO+1 (LUMO+2 for **3**) is a strongly σ-antibonding orbital, which carries in-plane interactions formed by four sulfur p orbitals and the metal's d_{xy} orbital. LUMO+2 (LUMO+1 for **3**) is a maleonitriledithiolate-based π^* orbital of a local a_2 symmetry. The existence of a relatively low-lying orbital localized on the *pull* ligand[6] is reported to be involved in a dithiolate-based emitting state in certain [Pt(diimine)(dithiolate)] complexes.[51,54]

On the basis of the provided shapes of the electron density plots (Figure 8) and data provided in Table 5, we conclude that the general electro-optical properties of **1**−**3** should not differ from those expected for *push*−*pull* complexes. On the other hand, the difference in the central metal should induce differences not only to their structure (vide infra) but also to their properties. Focusing our attention on the HOMO and LUMO, it is evident that LUMO's energy is almost stable along the series. In other words, the three compounds should have an almost identical reduction potential. On the other hand, the HOMO is more delocalized in **3** than in **1** and **2**, with the metal contribution maximized at the former complex. Thus, **3** is expected to be easier oxidized than **1** and **2**, a fact that is verified by our experimental results (see Table 2). The same trend was observed recently for the [M(Bz_2pipdt)(mnt)] series.[6]

Although the electronic differences between the syn and the anti isomers of **1**−**3** are expected to have a minor impact on the compounds' solution properties, it is worth mentioning some observed trends. First, orbitals that are localized mainly on the M(mnt) moiety, such as the HOMO, keeping their energy stable. Second, the LUMO, which is localized on the dithione but also raised by M(mnt)'s electron back-donation to it, is destabilized in the *b* conformers (the anti ones) as compared to the *a* ones (the syn ones) in all solvents and also in the gas phase. As a result, the HOMO−LUMO gap of the anti conformer is in any case slightly larger. On the other hand, pure dithione orbitals, such as LUMO+3, are heavily stabilized in the anti isomers (**b**) of **1**−**3** as a result of the slightly larger twisting of the dithione ligand in the anti conformers, as shown by the values of the δ_2 torsion angle (Tables S7−S9, Supporting Information).

Complexes **3a** and **4**[8] have the same metal−dithiolate moiety, with the former having a diazepanedithione ligand and the latter a piperazinedithione one. Upon changing the ligand, the dithione-based LUMO is strongly stabilized, a fact that is in accordance with the structural characteristics of the two complexes (vide supra). This stabilization should cause an anodic shift to **4**'s reduction potential as compared to **3**'s. Our experimental results support this trend (E_{red}^{I} = −0.42 V for **3** and E_{red}^{I} = −0.37 V for **4**). Moreover, **4**'s HOMO is slightly stabilized as well. The piperazine ligand, as it was revealed by the aforementioned arguments, is a better π^* acceptor. In other words, it should accommodate better the extra charge back-donated to it and hence stabilize the HOMO as well. This is also supported by electrochemistry data (E_{ox} = +0.96 V for **3** and E_{ox} = +1.08 V for **4**). In addition, from a comparison between the two [M(Bz_2pipdt)(dithiolate)] complexes, namely, **4** and **5**, we observe that the HOMO is destabilized in **5**, a fact that is in total accordance with both structural (vide supra) and electrochemical results (E_{ox} = +1.08 V for **4** and E_{ox} = +0.86 V for **5**). This is a result of the lower electron-accepting ability of the dmit ligand as compared to mnt. From an orbital point of view, in **5**'s HOMO the dithiolate contribution is raised, mainly at the metal's expense. Finally, **5**'s LUMO is only slightly destabilized, and this trend is also observed in reduction potentials (E_{red}^{I} = −0.39 V[6]). The frontier orbitals of **4** and **5** are depicted in Figure 9.

c. Optical Properties. In order to reveal and describe the optical properties of compounds **1**−**3**, TDDFT calculations were performed. Chloroform and acetonitrile were employed since these compounds are highly solvatochromic. Selected data are summarized in Tables 6−8, whereas all data are provided in Tables S11−S22, Supporting Information. Care was taken in order for the aforementioned conformer analogies to be taken into account, and thus, energies and oscillator strengths were corrected accordingly. The transitions under study fulfill the criteria posed by Casida,[55] and the following abbreviations were employed: MMLL CT = mixed metal−ligand to ligand charge transfer, MLCT = metal to ligand charge transfer, LMCT = ligand to metal charge transfer, LLCT = ligand to ligand charge transfer, and IL = intra ligand charge transfer.

Complexes **1**−**3** exhibit a highly negatively solvatochromic band in the low-energy region of their spectrum [**1**, λ/nm (ε/dm^3 mol^{-1} cm^{-1}): 601 (2.4 × 10^3), 818 (1.9 × 10^3) in CH_3CN; **2**, 670 (1.0 × 10^3), and **3** 680 (7.1 × 10^3) in DMF], which is assigned as a mixed-metal−ligand-to-ligand charge-transfer transition $a^1A \rightarrow b^1A$ (MMLL'CT) and can be described up to a point as a HOMO → LUMO transition. This type of transition is usually linked to enhanced nonlinear optical properties, such as the relatively high values of molecular hyperpolarizability.[6,56] From a computational point of view, our TDDFT-derived energies are very close to the experimental ones. Among the three complexes, namely, **1**−**3**, the nickel's charge-transfer band is bathochromically shifted as

dx.doi.org/10.1021/ic402738b | Inorg. Chem. 2014, 53, 1170−1183

Table 5. Contribution of Different Fragments to Complexes Valence Orbitals[a]

MO	E_{eV}	dithione	M	dithiolate	MO	E_{eV}	dithione	M	dithiolate
		1a in $CHCl_3$					**3a** in CH_3CN		
		unoccupied					unoccupied		
107	−0.47	6.9	10.8	82.2	107	−0.61	0.5	11.2	88.3
106	−1.40	93.0	5.1	1.9	106	−1.19	94.2	4.5	1.3
105	−1.95	1.6	1.6	96.7	105	−1.79	30.5	33.6	35.9
104	−2.33	27.5	43.3	29.2	104	−2.17	0.2	2.2	97.6
103	**−3.40**	**87.5**	**6.3**	**6.2**	**103**	**−3.36**	**89.5**	**5.0**	**5.5**
		occupied					occupied		
102	**−5.58**	**9.5**	**13.8**	**76.7**	**102**	**−5.54**	**15.1**	**19.3**	**65.6**
101	−6.56	19.4	46.9	33.7	101	−6.34	32.3	40.4	27.3
100	−6.73	4.7	83.4	11.9	100	−6.86	5.5	84.7	9.8
99	−7.15	45.2	21.9	33.0	99	−7.17	41.8	25.2	33.0
98	−7.18	38.0	32.5	29.5	98	−7.42	50.5	4.3	45.2
97	−7.40	36.4	8.9	54.8	97	−7.54	48.1	6.5	45.4
		1a in CH_3CN					**4** in CH_3CN		
		unoccupied					unoccupied		
107	−0.67	7.0	4.0	89.0	135	−0.77	98.1	1.4	0.6
106	−1.31	93.5	5.4	1.1	134	−0.84	97.8	0.9	1.3
105	−2.18	0.9	1.5	97.7	133	−1.89	29.7	33.8	36.4
104	−2.37	30.7	41.8	27.5	132	−2.22	0.1	2.3	97.6
103	**−3.28**	**86.3**	**7.9**	**5.8**	**131**	**−3.56**	**88.3**	**5.3**	**6.4**
		occupied					occupied		
102	**−5.70**	**9.6**	**15.1**	**75.2**	**130**	**−5.67**	**17.7**	**16.4**	**65.9**
101	−6.60	31.3	48.5	20.2	129	−6.49	31.9	38.4	29.7
100	−6.77	3.5	84.9	11.5	128	−7.03	11.6	82.3	6.2
99	−7.18	46.2	10.4	43.5	127	−7.17	90.6	6.5	2.9
98	−7.22	35.1	37.2	27.8	126	−7.18	94.2	1.6	4.2
97	−7.45	40.6	7.0	52.4	125	−7.32	99.3	0.4	0.3
		2a in CH_3CN					**5** in CH_3CN		
		unoccupied					unoccupied		
107	−0.63	−2.3	14.1	88.2	149	−0.80	15.1	3.5	81.4
106	−1.40	94.9	4.1	0.9	148	−0.91	98.2	0.7	1.0
105	−2.16	0.2	1.6	98.2	147	−1.77	30.8	34.7	34.5
104	−2.39	38.5	30.6	30.9	146	−2.13	0.0	0.2	99.8
103	**−3.28**	**83.4**	**8.1**	**8.5**	**145**	**−3.50**	**85.2**	**5.6**	**9.2**
		occupied					occupied		
102	**−5.65**	**8.4**	**14.0**	**77.6**	**144**	**−5.24**	**15.1**	**8.8**	**76.1**
101	−6.59	37.7	35.9	26.4	143	−6.19	21.9	35.2	42.9
100	−6.93	4.8	75.2	20.0	142	−6.49	18.8	21.1	60.1
99	−7.27	51.2	21.0	27.8	141	−6.52	1.2	0.5	98.4
98	−7.32	47.9	9.4	42.7	140	−6.91	6.3	86.5	7.2
97	−7.41	50.3	5.1	44.6	139	−7.10	66.5	1.0	32.5

[a]HOMO and LUMO orbitals are shown in bold.

compared to **2**'s and **3**'s, with the energy of the CT band to increase along the series Ni < Pt ≈ Pd in acetonitrile but along the series Ni < Pd ≈ Pt in the less polar chloroform. The former series is also observed in polar solvents in the relative compounds [M(Bz_2pipdt)(mnt)], M = Ni, Pd, Pt.[6] Moreover, the platinum compound owns the more intense charge-transfer band among the three, which is predicted also by the higher oscillator strength. This is reflected in the NLO properties of these compounds since the oscillator strength connects with the transition dipole moment.

The second interesting feature that we should comment on is that in the low-energy region of the spectrum there are two distinct negatively solvatochromic bands observed in **2** (in all solvents but not chloroform, in which one band and a shoulder is observed) but only one for **3**. This represents another difference with the relative [Pd(Bz_2pipdt)(mnt)],[6] since in the latter the second band is only a shoulder. There is only one band in **3** because in its case the relative transition owns smaller oscillator strength than the nonsolvatochromic transition $a^1A \rightarrow f^1A$, and its band is absorbed into it. Lastly, we should comment on nickel's absorption spectra. Its two bands own a strong multiconfigurational character, since the same two transitions contribute to the final states, HOMO → LUMO (MMLL′CT) and HOMO → LUMO+1 (LMCT/LLCT). Again, **1** has two distinct bands as compared to the one band and a shoulder observed in [Ni(Bz_2pipdt)(mnt)].[6,9]

In order to gain more insight into the role of the ligands we employed TD calculations also for complexes **4** and **5**. Derived results are summarized in Tables 9 and 10 and fully provided in Tables S23 and 24, Supporting Information.

Taking the whole series into account, we observe that in a polar solvent, such as acetonitrile, the energy of the main

dx.doi.org/10.1021/ic402738b | Inorg. Chem. 2014, 53, 1170−1183

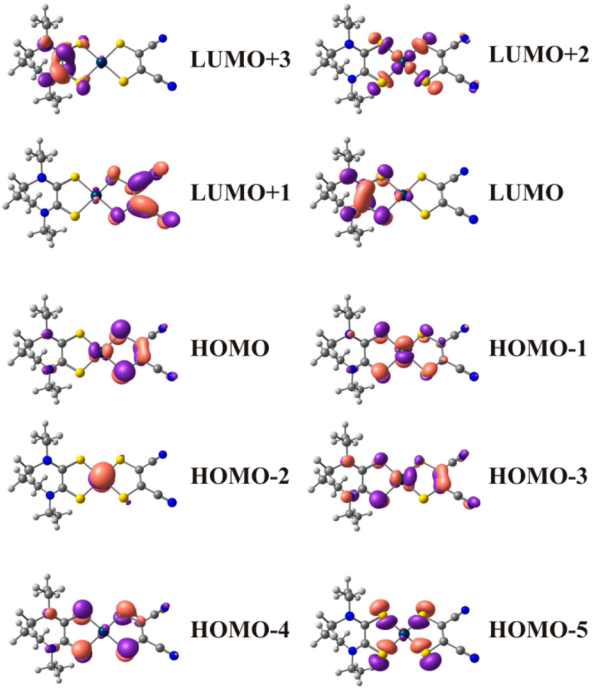

Figure 8. 0.052 au contour plots of the frontier orbitals of **3a**.

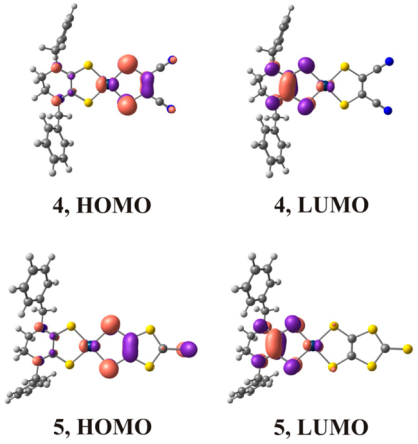

Figure 9. 0.05 au contour plots of the frontier orbitals of **4** and **5**.

MMLL′CT band is red shifted in the order **4** > **3** > **5** while the oscillator strength increases in the order **3** < **4** < **5**. In other words, the [Pt(Bz$_2$pipdt)(dmit)] complex, **5**, has the smallest transition energy along the series but the largest oscillator strength. Hence, **5** is anticipated to have the largest molecular hyperpolarizability along the series and as a result should be the best candidate for application in NLO materials. The latter argument can be described also in terms of the simple two-state model.[57] Accordingly, the hyperpolarizability of a compound, which has only two significant states, the ground and the first exited states, is provided by eq 1a

$$\beta_{CT} - \frac{(\mu_e - \mu_g)\mu_{ge}^2}{\Delta E_{ge}^2} \tag{1a}$$

where μ_e is the excited-state dipole moment, μ_g is the ground state dipole moment, μ_{ge} is the transition state dipole moment, and ΔE_{ge} is the transition energy between the two states.

A comparison of the absorption spectra between **3** and **4** further reveals the influence of the structural changes on the electronic properties of these complexes. As already indicated, replacement of the piperazine ligand with the diazepane induces a significant twist in the dithione structure (see δ_1 and δ_2 values in Tables S3− S5, Supporting Information). As a result, the worse the overlap between the orbitals that contribute to the final states, the lower the oscillator strength of the main charge-transfer band (**3** < **4** < **5**). The larger oscillator strength of **5** vs **4** is dependent both on the larger torsion angles of **4** and the extent of the π-orbital system of the 2-thioxo-1,3-dithiole-4,5-bis(thiolate).

4. MOLECULAR HYPERPOLARIZABILITIES

In order to elucidate the compounds' second-order response and complement our EFISH results, computation of the static and dynamic hyperpolarizabilities according to the coupled perturbed Kohn−Sham methodology was employed together with the polarizable conductor calculation model (CPCM). Acetonitrile is a polar solvent and anticipated to induce analogous solvation interactions to DMF, which was the solvent employed in our EFISH experiments. In additiont, we selected 0.65 eV to be our theoretical laser fundamental radiation, which was also used throughout the experimental procedure.

Table 6. TDDFT-Calculated Energies and Compositions of the Most Important Singlet Electronic Transitions of 1[a]

state	composition[b]	ΔE[c]	exp.[d]	f[e]	character
B^{1}A	**HOMO → LUMO, 56 (*44*) %**	**1.42**	**1.41**	**0.0590**	**MNT/NI → ET$_2$dazdt (MMLL′CT)**
	HOMO → LUMO+1, 29 (*35*)%	***1.45***	***1.51***	***0.0331***	**MNT/NI → NI/MNT/ET$_2$DAZDT (LMCT/LLCT)**
E^{1}A	HOMO → LUMO, 44 (*55*) %	1.94	1.91	0.1391	MNT/NI → ET$_2$DAZDT (MMLL′CT)
	HOMO → LUMO+1, 29 (*31*)%	*2.09*	*2.07*	*0.1693*	MNT/NI → NI/MNT/ET$_2$DAZDT (LMCT/LLCT)
K^{1}A	HOMO-5 → LUMO, 79%	3.16[f]		0.0783	MNT/ET$_2$DAZDT → ET$_2$DAZDT (MMLL′CT)
L^{1}A	HOMO → LUMO+2, 45 (*89*)%		2.99		MNT/NI → MNT (ILCT)
	HOMO-3 → LUMO, 23%	3.18[f]	*2.99*	0.1212	ET$_2$DAZDT/MNT/NI → ET$_2$DAZDT
J^{1}A	HOMO-4 → LUMO, 18%	*2.99*[f]		*0.1418*	ET$_2$DAZDT/MNT/NI → ET$_2$DAZDT

[a]Principal singlet transition responsible for the main absorption band in the visible region is shown in bold. Data in plain text correspond to chloroform's field, while data in italics correspond to acetonitrile's field. [b]Compositions of electronic transitions are expressed in terms of contributing excitations between ground-state Kohn−Sham molecular orbitals. Only the syn conformers are reported. [c]Transition energy from the a^{1}A ground state in eV. Theoretical values provided are weighted mean values based on the contributions from the two conformers provided in Table 4. [d]Values for a $CHCl_3$ solution are in plain text, while CH_3CN values are in italics. [e]Oscillator strength. Theoretical values provided are weighted mean values based on the contributions from the two conformers provided in Table 4. [f]Simulation of the theoretical spectra with the appropriate broadening model of the bands provide the value of 2.99 eV as a shoulder to ∼300 nm main peak.

dx.doi.org/10.1021/ic402738b | Inorg. Chem. 2014, 53, 1170−1183

Table 7. TDDFT-Calculated Energies and Compositions of the Most Important Singlet Electronic Transitions of 2[a]

state	composition[b]	ΔE[c]	exp.[d]	f[e]	character
B^{1}A	**HOMO → LUMO, 92 (*88*) %**	**1.53**	**1.51**	**0.0936**	**MNT/PD → ET$_2$DAZDT (MMLL′CT)**
	HOMO → LUMO+1, 8 (*11*) %	***1.68***	***1.86***	***0.0795***	**MNT/PD → ET$_2$DAZDT/MNT/PD (LMCT/LLCT)**
C^{1}A	HOMO → LUMO+1, 90 (*87*) %	2.20	1.94	0.0583	MNT/PD → ET$_2$DAZDT/MNT/PD (LMCT/LLCT)
	HOMO → LUMO, 8 (*11*) %	*2.33*	*2.56*		MNT/PD → ET$_2$DAZDT (MMLL′CT)
G^{1}A	HOMO → LUMO+2, 62%	3.04	2.87	0.0626	MNT/PD → MNT (ILCT/MLCT)
	HOMO-2 → LUMO+1, 12%				PD/MNT → ET$_2$DAZDT/MNT/PD (MLCT/ML′CT)
	HOMO-1 → LUMO+1, 15%				MNT/PD/ET$_2$DAZDT → ET$_2$DAZDT/MNT/PD
F^{1}A	*HOMO → LUMO+2, 80%*	*2.98*	*3.00*	*0.1089*	*MNT/PD → MNT (ILCT)*
	HOMO-2 → LUMO, 10%				*PD/MNT → ET$_2$DAZD (MLCT/LL CT)*
E^{1}A	HOMO-3 → LUMO, 55%	3.14	3.42	0.1993	MNT/PD → ET$_2$DAZDT/MNT/PD (LMCT/LLCT)
	HOMO-5 → LUMO, 23%				MNT/PD → ET$_2$DAZDT (MMLL′CT)
	HOMO-4 → LUMO, 15%				ET$_2$DAZDT/MNT/PD → ET$_2$DAZDT (ILCT/LLCT)
H^{1}A	*HOMO-3 → LUMO, 79%*	*3.26*	*3.47*	*0.2106*	*ET$_2$DAZDT/MNT/PD → ET$_2$DAZDT (ILCT/LLCT)*

[a]Principal singlet transition responsible for the main absorption band in the visible region is shown in bold. Data in plain text correspond to chloroform's field, while data in italics correspond to acetonitrile's field. [b]Compositions of electronic transitions are expressed in terms of contributing excitations between ground-state Kohn−Sham molecular orbitals. Only the syn conformer's are reported. [c]Transition energy from the a^{1}A ground state in eV. Theoretical values provided are weighted mean values based on the contributions from the two conformers provided in Table 4. [d]Values for a $CHCl_3$ solution are in plain text, while CH_3CN values are in italics. [e]Oscillator strength. Theoretical values provided are weighted mean values based on the contributions from the two conformers provided in Table 4.

Table 8. TDDFT-Calculated Energies and Compositions of the Most Important Singlet Electronic Transitions of 3[a]

state	composition[b]	ΔE[c]	exp.[d]	f[e]	character
B^{1}A	**HOMO → LUMO, 99 (*98*) %**	***1.57*** (***1.67***)	***1.52*** (***1.81***)	***0.2490*** (***0.2465***)	**MNT/PT/ET$_2$DAZDT → ET$_2$DAZDT**
		1.67	1.81	0.2465	
E^{1}A	HOMO → LUMO+2, 97%	2.69	2.72SH	0.0237	MNT/PT/ET$_2$DAZDT → MNT/PT/ET$_2$DAZDT
F^{1}A	HOMO → LUMO+1, 93 (*96*) %	3.01	*2.80*	0.0925	MNT/PT/ET$_2$DAZDT → MNT(ILCT/LLCT)
		2.84		*0.1254*	
G^{1}A	HOMO-3 → LUMO, 85 (*92*) %	3.11	3.43	0.1201	ET$_2$DAZDT/PT/MNT → ET$_2$DAZDT
		3.22	*3.11*	*0.1529*	
N^{1}A	HOMO-1 → LUMO+1, 92 (*95*) %	3.79	3.97	0.1979	PT/ET$_2$DAZDT/MNT → MNT (MMLL′CT)
K^{1}A		*3.59*	*3.75*	*0.1868*	

[a]Principal singlet transition responsible for the main absorption band in the visible region is shown in bold. Data in plain text correspond to chloroform's field, while data in italics correspond to acetonitrile's field. [b]Compositions of electronic transitions are expressed in terms of contributing excitations between ground-state Kohn−Sham molecular orbitals. Only the syn conformers are reported. [c]Transition energy from the a^{1}A ground state in eV. Theoretical values provided are weighted mean values based on the contributions from the two conformers provided in Table 4. [d]Values for $CHCl_3$ solution are in plain text, while CH_3CN values are in italics. [e]Oscillator strength. Theoretical values provided are weighted mean values based on the contributions from the two conformers provided in Table 4.

Table 9. TDDFT-Calculated Energies and Compositions of the Most Important Singlet Electronic Transitions of 4[a]

state	composition[b]	ΔE[c]	exp.[d]	f[e]	character
b^{1}A	**HOMO → LUMO, *100*%**	**1.71**	**1.87**	**0.3795**	**MNT/PT/BZ$_2$PIPDT → BZ$_2$PIPDT**
F^{1}A	HOMO → LUMO+1, *94* %	2.94	2.38sh	0.1197	MNT/PT/BZ$_2$PIPDT → MNT (ILCT/LLCT)
K^{1}A	HOMO-7 → LUMO, *93* %	3.22	3.16	0.1356	BZ$_2$PIPDT/MNT/PT→ ET$_2$DAZDT
P^{1}A	HOMO-1 → LUMO+1, *96* %	3.70	3.62	0.1893	PT/BZ$_2$PIPDT/MNT → MNT (MMLL′CT)

[a]Principal singlet transition responsible for the main absorption band in the visible region is shown in bold. [b]Compositions of electronic transitions are expressed in terms of contributing excitations between ground-state Kohn−Sham molecular orbitals. [c]Transition energy from the a^{1}A ground state in eV as was calculated in acetonitrile's field. [d]Values for a CH_3CN solution. [e]Oscillator strength.

Table 10. TDDFT-Calculated Energies and Compositions of the Most Important Singlet Electronic Transitions of 5[a]

state	composition[b]	ΔE[c]	exp.[d]	f[e]	character
B^{1}A	**HOMO → LUMO, *100*%**	**1.38**	**1.50**	**0.4477**	**DMIT/PT/BZ$_2$PIPDT → BZ$_2$PIPDT (MMLL′CT)**
F^{1}A	HOMO → LUMO+1, *59* %	2.55	2.57	0.1742	DMIT/PT/BZ$_2$PIPDT → MNT (ILCT/LLCT)
	HOMO → LUMO+2, *28* %				DMIT/PT/BZ$_2$PIPDT → PT/DMIT/BZ$_2$PIPDT
	HOMO-2 → LUMO, *11* %				DMIT/PT/BZ$_2$PIPDT → BZ$_2$PIPDT (MMLL′CT)

[a]Principal singlet transition responsible for the main absorption band in the visible region is shown in bold. [b]Compositions of electronic transitions are expressed in terms of contributing excitations between ground-state Kohn−Sham molecular orbitals. [c]Transition energy from the a^{1}A ground state in eV as calculated in acetonitrile's field. [d]Values for a DMF solution taken from refs 6 and 36. [e]Oscillator strength.

dx.doi.org/10.1021/ic402738b | Inorg. Chem. 2014, 53, 1170−1183

Table 11. Experimental and Calculated Hyperpolarizability Values for 1−5

complex	$\mu\beta_\lambda^{exp}(10^{-48}$ esu)	$\mu\beta_0^{exp}(10^{-48}$ esu)	β_{vec} $(10^{-30}$ esu)	β_{vec} $\hbar\omega$ = 0.65 eV $(10^{-48}$ esu)	μ (D)	$\mu\beta_{vec}$ $(10^{-48}$ esu)	$\mu\beta_{vec}$ *with* $\hbar\omega$ = 0.65 eV $(10^{-48}$ esu)
1	*(−900)*[a]	*(−212)*[a]	−24.4	−20.6	37.6	−916.9	−773.3
2	−400	−177	−17.3	−15.0	38.4	−664.3	−573.44
3	−1300	−576	−37.1	−29.8	37.7	−1397.5	−1121.5
4	−1950	−822	−45.4	33.1	35.3	−1603.1	−1168.2
5	−10000	−2011	−146.4	116.2	32.3	−4726.3	−3751.6

[a]On standing a change to yellow of the green DMF solution of **1** appears.

The first hyperpolarizabilities of **1**−**3** were calculated only for the syn conformers. In addition, we performed analogous calculations for **4** and **5**. Our model works according to the following equations, and the results for both static and dynamic β are provided in Table 11.

$$\beta_i = \beta_{iii} + \frac{1}{3}\sum_{i\neq k}(\beta_{ikk} + \beta_{kik} + \beta_{kki}), \text{ with } i, k = x, y, z \quad (2)$$

$$\beta_{vec} = \frac{\mu_i\beta_i}{\mu_g} \quad (3)$$

Since it is well known that coupled perturbed calculations do not afford beta values that coincide accurately to the experimental ones, trying to judge the validity of our calculations we employed a regression analysis. Thus, in Figure 9 the experimental beta values for the four complexes **2**−**5** are related to the calculated ones. As can be seen from Figure 10, a correlation between theoretical and EFISH results can be characterized as very satisfactory.

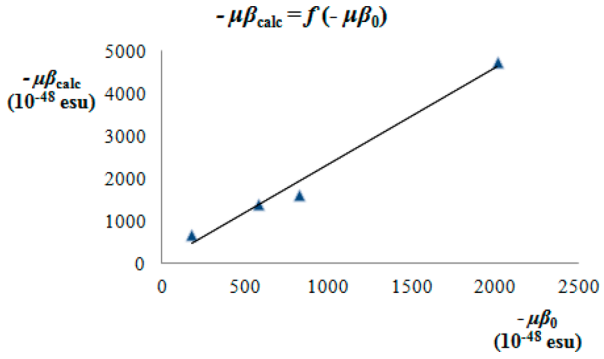

Figure 10. Graphic representation of the function $\mu\beta_0^{exp} = f(\mu\beta_0^{calcd})$. Pearson's coefficient for the equation $-\mu\beta_0^{exp} = 2.2602(-\mu\beta_0^{calcd}) + 71.506$ is $R^2 = 0.98$.

However, **2** and **3** along with **1**, according to our calculations, show second-order response. In particular, **3** shows the largest beta values along this series. The same trend was recently observed in the relative [M(Bz_2pipdt)(dmit)] series[8] and to other *push*−*pull* complexes[58,59] as well. On the other hand, according to our calculations it seems that **1** has slightly larger beta values as compared to **2**, in contrast to the piperazine compounds. Unfortunately **1** decomposes in DMF, and thus, the obtained values can be considered only as a rough approximation. Thus, it was not possible to check this argument experimentally in a fully reliable way.

The order of the values of $\mu\beta_0$ for complexes **2**−**5** is **5** > **4** > **3** > **2**. This is opposite to the order of the δ_2 torsion angle of these complexes, revealing the role of the dithione ligands and the metal not only to the structure of these complexes but also to their properties. The superiority of **5** on NLO properties must also be attributed to the extent of the π system of the dithiolate ligand, namely, 2-thioxo-1,3-dithiolane-4,5-dithiolate.

CONCLUSIONS

Combined experimental and theoretical studies on [M(II)-(Et_2dazdt)(mnt)] (M = Ni, **1**; Pd, **2**; Pt, **3**) [Et_2dazdt = *N*,*N*′-diethyl-perhydrodiazepine-2,3-dithione; mnt = maleonitrile-2,3-dithiolate], which are redox-active complexes and exhibit negative molecular quadratic optical nonlinearities, have been performed to highlight the role of the acceptor ligand in the NLO properties of the donor−acceptor metal-d[8] dithiolene triad [M(II)(dithione)(dithiolate)]. Accordingly, structural, electrochemical, spectroscopic, and EFISH data as well as DFT and TD-DFT including CPCM methods were employed to study **1**−**3** to gain further insight into the structure−property relationships. The same computational methods were also employed for the strictly related complex [Pt(Bz_2pipdt)(mnt)] (**4**)[6] and [Pt(Bz_2pipdt)(dmit)] (**5**), which exhibits the largest second-order NLO activity so far determined for this class of complexes. Results of theoretical calculations on **1**−**5** reveal that the structural properties of the complexes strongly affect the electronic and NLO properties of this class of complexes. Actually, the order of the dithione torsion angle δ_2 for complexes **2**−**5** is **2** > **3** > **4** > **5** correlates inversely with the oscillator strength and $\mu\beta_0$ (**5** > **4** > **3** > **2**).

Moreover, analysis of the factors which affect NLO activity shows that the remarkable first molecular hyperpolarizability of **5** can be attributed both to its lowest torsion angles and to the π system extent of its dithiolate ligand, dmit, which confirms it to behave as an optimal candidate as donor in donor−acceptor mixed-ligand dithiolene complexes to achieve high second-order NLO activity.

ASSOCIATED CONTENT

Supporting Information

Experimental and calculated structural parameters for **1**−**5**; contribution of different fragments to complexes' valence orbitals; TDDFT results for complexes under study; cyclic voltammetry full scan for **3**; two conformations; fingerprint plots. This material is available free of charge via the Internet at http://pubs.acs.org.

AUTHOR INFORMATION

Corresponding Authors

*E-mail: cmitsop@chem.uoa.gr.
*E-mail: deplano@unica.it.

Notes

The authors declare no competing financial interest.

dx.doi.org/10.1021/ic402738b | *Inorg. Chem.* 2014, 53, 1170−1183

■ ACKNOWLEDGMENTS

This research was performed inside the Project "Composti funzionali basati su complessi di metalli di transizione per applicazioni High-Tech" supported by Fondazione Banco di Sardegna and Università di Cagliari. We thank Chin-Ti Chen, Research Fellow of the Institute of Chemistry, Academia Sinica, and Prof. Chih-Chieh Wang, Department of Chemistry, Soochow University, for providing us with the crystal structure of **1**. Preliminary experiments for samples preparation have been performed by Mirko Vacca during his research stage for his bachelor's degree. Thanks are also due to COST Actions for supporting cooperation between P. D. and C. A. M. groups. This cooperation started during COST Action D35 and is going on in the new COST Action CM1202, PERSPECT-H2O Supramolecular photocatalytic water splitting.

■ REFERENCES

(1) (a) McNamara, W. R.; Han, Z.; Yin, C.-J.; Brennessel, W. W.; Holland, P. L.; Eisenberg, R. *Proc. Natl. Acad. Sci. U.S.A.* **2012**, *109*, 15594. (b) Chang, C. C.; Pfenning, B.; Bocarsly, A. B. *Coord. Chem. Rev.* **2001**, *211*, 195.

(2) (a) Zhang, J.; Du, P.; Schneider, J.; Jarosz, P.; Eisenberg, R. *J. Am. Chem. Soc.* **2007**, *129*, 772. (b) Dalgleish, S.; Labram, J. G.; Li, Z.; Wang, J.; McNeil, C. R.; Anthopoulos, T. D.; Greenham, N.; Robertson, N. *J. Mater. Chem.* **2011**, *21*, 15422.

(3) (a) Cariati, E.; Pizzotti, M.; Roberto, D.; Tessore, F.; Ugo, R. *Coord. Chem. Rev.* **2006**, *250*, 1210−1233. (b) Di Bella, S.; Dragonetti, C.; Pizzotti, M.; Roberto, D.; Tessore, F.; Ugo, R. In *Molecular Organometallic Materials for Optics−Topics in Organometallic Chemistry*; Le Bozec, H., Guerchais, V., Eds.; Springer-Verlag: Berlin, Heidelberg, 2010; Vol. *28*, pp 1−55.

(4) (a) Deplano, P.; Mercuri, M. L.; Serpe, A.; Pilia, L. Structure and Properties of *d8*-Metal Dithiolene Complexes. In *The chemistry of metal enolates*; Zabicky, J., Ed.; Wiley & Sons, Ltd.: New York, 2009; Chapter 16, pp 879−928. (b) Deplano, P.; Pilia, L.; Espa, D.; Mercuri, M. L.; Serpe, A. *Coord. Chem. Rev.* **2010**, *254*, 1434.

(5) (a) Chen, C. T.; Liao, S. Y.; Lin, K. J.; Lai, L. L. *Adv. Mater.* **1998**, *3*, 335. (b) Bigoli, F.; Chen, C. T.; Deplano, P.; Mercuri, M. L.; Pellinghelli, M. A.; Pilia, L.; Pintus, G.; Serpe, A.; Trogu, E. F. *Chem. Commun.* **2001**, 2246. (c) Curreli, S.; Deplano, P.; Faulmann, C.; Ienco, A.; Mealli, C.; Mercuri, M. L.; Pilia, L.; Pintus, G.; Serpe, A.; Trogu, E. F. *Inorg. Chem.* **2004**, *43*, 5069.

(6) Pilia, L.; Espa, D.; Barsella, A.; Fort, A.; Mitsopoulou, C. A.; Marchiò, L.; Mercuri, M. L.; Serpe, A.; Makedonas, C.; Deplano, P. *Inorg. Chem.* **2011**, *50*, 10015.

(7) Isaksson, R.; Lijefors, T.; Sandstrom, J. *J. Chem. Res. Miniprint* **1981**, 664.

(8) Espa, D.; Pilia, L.; Marchiò, L.; Mercuri, M. L.; Serpe, A.; Barsella, A.; Fort, A.; Dalgleish, S.; Robertson, N.; Deplano, P. *Inorg. Chem.* **2011**, *50*, 2058.

(9) Espa, D.; Pilia, L.; Marchiò, L.; Artizzu, F.; Mercuri, M. L.; Serpe, A.; Simão, D.; Almeida, M.; Pizzotti, M.; Tessore, F.; Deplano, P. *Dalton Trans.* **2012**, *41*, 3485.

(10) *SMART (control) and SAINT (integration) software for CCD systems*; Bruker AXS: Madison, WI, 1994.

(11) *Area-Detector Absorption Correction*; Siemens Industrial Automation, Inc.: Madison, WI, 1996.

(12) Altomare, A.; Burla, M. C.; Camalli, M.; Cascarano, G. L.; Giacovazzo, C.; Guagliardi, A.; Moliterni, A. G. G.; Polidori, G.; Spagna, R. *J. Appl. Crystallogr.* **1999**, *32*, 115.

(13) Burla, M. C.; Caliandro, R.; Camalli, M.; Carrozzini, B.; Cascarano, G. L.; De Caro, L.; Giacovazzo, C.; Polidori, G.; Spagna, R. *J. Appl. Crystallogr.* **2005**, *38*, 381.

(14) Sheldrick, G. M. *SHELX97. Programs for Crystal Structure Analysis*, Release 97-2; University of Göttingen: Germany, 1997.

(15) Farrugia, L. J. *J. Appl. Crystallogr.* **1999**, *32*, 837.

(16) (a) Farrugia, L. J. *J. Appl. Crystallogr.* **1997**, *30*, 568. (b) Macrae, C. F.; Bruno, I. J.; Chisholm, J. A.; Edgington, P. R.; McCabe, P.; Pidcock, E.; Rodriguez-Monge, L.; Taylor, R.; van de Streek, J.; Wood, P. A. *J. Appl. Crystallogr.* **2008**, *41*, 466.

(17) (a) Spackman, M. A.; Jayatilaka, D. *CrystEngComm* **2009**, *11*, 19. (b) Wolff, S. K.; Grimwood, D. J.; McKinnon, J. J.; Turner, M. J.; Jayatilaka, D.; Spackman, M. A. *CrystalExplorer*; University of Western Australia: Perth, 2012.

(18) Parr, R. G.; Yang, W. *Density Functional Theory of Atoms and Molecules*; Oxford University Press: Oxford, 1989.

(19) Koch, W.; Holthausen, M. C. *A Chemist's Guide to Density Functional Theory*; Wiley-VCH Verlag GmbH: Weinheim, 2000.

(20) Frisch, M. J.; Trucks, G. W.; Schlegel,H. B.; Scuseria, G. E.; Robb, M. A.; Cheeseman, J. R.; Scalmani, G.; Barone, V.; Mennucci, B.; Petersson, G. A.; Nakatsuji, H.; Caricato, M.; Li, X.; Hratchian, H. P.; Izmaylov, A. F.; Bloino, J.; Zheng, G.; Sonnenberg, J. L.; Hada, M.; Ehara, M.; Toyota, K.; Fukuda, R.; Hasegawa, J.; Ishida, M.; Nakajima, T.; Honda, Y.; Kitao, O.; Nakai, H.; Vreven, T.; Montgomery, J. A., Jr.; Peralta, J. E.; Ogliaro, F.; Bearpark, M.; Heyd, J. J.; Brothers, E.; Kudin, K. N.; Staroverov, V. N.; Kobayashi, R.; Normand, J.; Raghavachari, K.; Rendell, A.; Burant, J. C.; Iyengar, S. S.; Tomasi, J.; Cossi, M.; Rega, N.; Millam, N. J.; Klene, M.; Knox, J. E.; Cross, J. B.; Bakken, V.; Adamo, C.; Jaramillo, J.; Gomperts, R.; Stratmann, R. E.; Yazyev, O.; Austin, A. J.; Cammi, R.; Pomelli, C.; Ochterski, J. W.; Martin, R. L.; Morokuma, K.; Zakrzewski, V. G.; Voth, G. A.; Salvador, P.; Dannenberg, J. J.; Dapprich, S.; Daniels, A. D.; Farkas, O.; Foresman, J. B.; Ortiz, J. V.; Cioslowski, J.; Fox, D. J. *Gaussian 09*, Revision C.1; Gaussian, Inc.: Wallingford, CT, 2010.

(21) Becke, A. D. *J. Chem. Phys.* **1993**, *98*, 5648.

(22) Lee, C.; Yang, W.; Parr, R. G. *Phys. Rev. B* **1988**, *37*, 785.

(23) Krishnan, R.; Binkley, J. S.; Seeger, R.; Pople, J. A. *J. Chem. Phys.* **1980**, *72*, 650.

(24) McLean, A. D.; Chandler, G. S. *J. Chem. Phys.* **1980**, *72*, 5639.

(25) Woon, D. E.; Dunning, J. T. H. *J. Chem. Phys.* **1993**, *98*, 1358.

(26) Andra, D.; Häußermann, U.; Dolg, M.; Stoll, H.; Preuß, H. *Theor. Chim. Acta* **1990**, *77*, 123.

(27) Dolg, M.; Wetig, U.; Stoll, H.; Preuss, H. *J. Chem. Phys.* **1987**, *86*, 866.

(28) Figgen, D.; Peterson, K. A.; Dolg, M.; Stoll, H. *J. Chem. Phys.* **2009**, *130*, 164108.

(29) Martin, J. M. L.; Sunderman, A. *J. Chem. Phys.* **2001**, *114*, 3408.

(30) Peterson, K. A.; Figgen, D.; Dolg, M.; Stoll, H. *J. Chem. Phys.* **2007**, *126*, 124101.

(31) Gorelsky, S. I. *AOMix: Program for Molecular Orbital Analysis*, revision 6.60; University of Ottawa: Ottawa, Canada, 2012; http://www.sg-chem.net/.

(32) Gorelsky, S. I.; Lever, A. B. P. *J. Organomet. Chem.* **2001**, *635*, 187.

(33) Barone, V.; Cossi, M. *J. Phys. Chem. A* **1998**, *102*, 1995.

(34) Cossi, M.; Rega, N.; Scalmani, G.; Barone, V. *J. Comput. Chem.* **2003**, *24*, 669.

(35) Stratmann, R. E.; Scuseria, G. E.; Frisch, M. J. *J. Chem. Phys.* **1998**, *109*, 8218.

(36) Gorelsky, S. I. *SWizard program*, revision 4.6; http://www.sg-chem.net/.

(37) Willets, A.; Rice, J. E.; Burland, D. M. *J. Chem. Phys.* **1992**, *97*, 7590.

(38) Reis, H. *J. Chem. Phys.* **2006**, *125*, 014506.

(39) Zhurko, G. A.; Zhurko, D. A. *ChemCraft, Tool for treatment of the chemical data*, version 1.6; www.chemcraftprog.com.

(40) *Mercury*, Version 3.0.1; Cambridge Crystallographic Data Center: Cambridge, 2011.

(41) (a) Espa, D.; Pilia, L.; Marchiò, L.; Mercuri, M. L.; Serpe, A.; Sessini, E.; Deplano, P. *Dalton Trans.* **2013**, *42*, 12429. (b) Bigoli, F.; Deplano, P.; Mercuri, M. L.; Pellinghelli, M. A.; Pilia, L.; Pintus, G.; Serpe, A.; Trogu, E. F. *Inorg. Chem.* **2002**, *41*, 5241. (c) Deplano, P.; Mercuri, M. L.; Marchiò, L.; Pilia, L.; Salidu, M.; Serpe, A.; Congiu, F.; Sanna, S. *Eur. J. Inorg. Chem.* **2005**, 1829.

(42) (a) Cummings, S. D.; Eisenberg, R. *J. Am. Chem. Soc.* **1996**, *118*, 1949. (b) Cummings, S. D.; Cheng, L.-T.; Eisenberg, R. *Chem. Mater.* **1997**, *9*, 440. (c) Base, K.; Tierney, M. T.; Fort, A.; Muller, J.; Grinstaff, M. W. *Inorg. Chem.* **1999**, *38*, 287. (d) Mitsopoulou, C. A. *Coord. Chem. Rev.* **2010**, *254*, 1448.
(43) Wang, C. C.; Wu, W. C.; Lee, G. H.; Chen, C. T. *J. Chin. Chem. Soc.-Taip.* **2002**, *49*, 805.
(44) (a) Serpe, A.; Mercuri, M. L.; Pilia, L.; Deplano, P. *Coord. Chem. Rev.* **2008**, *252*, 1200. (b) Serpe, A.; Bigoli, F.; Cabras, M. C.; Deplano, P.; Fornasiero, P.; Graziani, M.; Mercuri, M. L.; Montini, T.; Pilia, L.; Trogu, E. F. *Chem. Commun.* **2005**, 1040.
(45) (a) Bigoli, F.; Angela Pellinghelli, M.; Deplano, P.; Laura Mercuri, M.; Pintus, G.; Serpe, A.; F. Trogu, E. *Chem. Commun.* **1998**, 2351. (b) Cau, L.; Deplano, P.; Marchio, L.; Mercuri, M. L.; Pilia, L.; Serpe, A.; Trogu, E. F. *Dalton Trans.* **2003**, 1969.
(46) Bigoli, F.; Cabras, M. C.; Deplano, P.; Mercuri, M. L.; Marchiò, L.; Serpe, A.; Trogu, E. F. *Eur. J. Inorg. Chem.* **2004**, 960.
(47) Freeman, F.; Hwang, J. H.; Junge, E. H.; Parmar, P. D.; Renz, Z.; Trinh, J. *Int. J. Quantum Chem.* **2008**, *108*, 339.
(48) Allen, F. H.; Howard, J. A. K.; Pitchford, N. A.; Vinter, J. G. *Acta Crystallogr.* **1994**, *B50*, 382.
(49) Bocian, D. F.; Strauss, H. L. *J. Am. Chem. Soc.* **1977**, *99*, 2876.
(50) Bocian, D. F.; Strauss, H. L. *J. Am. Chem. Soc.* **1977**, *99*, 2866.
(51) Makedonas, C.; Mitsopoulou, C. A.; Lahoz, F. J.; Balana, A. I. *Inorg. Chem.* **2003**, *42*, 8853.
(52) (a) Makedonas, C.; Mitsopoulou, C. A. *Inorg. Chim. Acta* **2007**, *360*, 3997. (b) Makedonas, C.; Mitsopoulou, C. A. *Spectrochim. Acta, Part A* **2006**, *64*, 918.
(53) Li, J.; Noodleman, L.; Case, D. A. In *Inorganic Electronic Stucture and Spectroscopy*; Solomon, E. I., Lever, A. B. P., Eds.; John Wiley & Sons: New York, 1999; Vol. *1*, pp 661−724.
(54) Zuleta, J. A.; Bevilacqua, J. M.; Eisenberg, R. *Coord. Chem. Rev.* **1991**, *111*, 237.
(55) Casida, M. E.; Jamorski, C.; Casida, K. C.; Salahub, D. R. *J. Chem. Phys.* **1998**, *108*, 4439.
(56) Cummings, S. D.; Cheng, L. T.; Eisenberg, R. *Chem. Mater.* **1997**, *9*, 440.
(57) (a) Oudar, J. L.; Chemla, D. S. *J. Chem. Phys.* **1977**, *66*, 2664. (b) Bruni, S.; Cariati, E.; Cariati, F.; Porta, F. A.; Quici, S.; Roberto, D. *Spectrochim. Acta, Part A* **2001**, *57*, 1417.
(58) Romaniello, P.; Lelj, F. *J. Mol. Struct. (THEOCHEM)* **2003**, *636*, 23.
(59) Romaniello, P.; Lelj, F. *J. Mol. Struct. (THEOCHEM)* **2003**, *372*, 51.